Remote Sensing of Environment xxx (xxxx) xxx–xxx

Contents lists available at ScienceDirect

Remote Sensing of Environment

journal homepage: www.elsevier.com/locate/rse

A satellite-derived climatology of unreported tornadoes in forested regions of northeast Europe

Andrey Shikhov[a,*], Alexander Chernokulsky[b]

[a] Department of Cartography and Geoinformatics, Perm State University, Perm, Russia
[b] A.M. Obukhov Institute of Atmospheric Physics, Russian Academy of Sciences, Moscow, Russia

ARTICLE INFO

Keywords:
Tornadoes
Tornado climatology
Tornado-induced forest damage
Satellite data
Landsat images
Global Forest Change data
Tornado outbreaks

ABSTRACT

This study presents a novel method of tornado track identification in forested regions in Europe based on remote sensing data. The method enables an objective estimate (i.e. independent of population density and observational networks) of tornado climatology in forested regions. The method is based on the identification of narrow and elongated areas as forest disturbances obtained using Landsat satellite images and Landsat-based Global Forest Change (GFC) data. These areas were subsequently verified with high-resolution satellite images for verification of a tornadic cause of forest damage. Landsat and MODIS satellite images, weather station observations and reanalysis data were additionally involved in order to determine tornado dates. A minimum F-scale tornado intensity was estimated by a Weibull distribution model using information on tornado path lengths and widths. The method is applied to the forested regions of northeast Europe, where 110 tornado tracks were identified between the 2000 and 2014 years, 105 of which were previously unreported and discovered for the first time. For some regions, tornado density estimates using the new method is 2–3 times higher than other previously published estimates. The largest number of tornadoes occurred in 2009, and June is the most favourable month for tornado formation (including strong tornadoes and tornado outbreaks). Most identified tornadoes have path length < 10 km with maximum and mean widths of approximately 200–300 m and 100–200 m, respectively. A few tornadoes with long and wide paths were found; four of them likely had F3 minimal intensity.

1. Introduction

Tornadoes are among the most destructive weather phenomena on the Earth, and have been observed on all continents except Antarctica (Goliger and Milford, 1998; Feuerstein et al., 2005).Tornadoes are reported more frequently in the United States (U.S.) where approximately 1000–1500 tornadoes are recorded per year (Coleman and Dixon, 2014). The maximum tornado frequency is found in the Midwestern U.S. (Coleman and Dixon, 2014; Rosencrants and Ashley, 2015), where up to 400 tornadoes per 10,000 km^2 were reported between 1950 and 2015 (Storm Prediction Center (SPC) Tornado Database; Schaefer and Edwards, 1999). Tornado frequency in Eurasia is significantly lower. According to the European severe weather database (ESWD) (Dotzek et al., 2009), 9529 tornadoes (over land and water) were recorded in Europe between 1800 and 2014 (Groenemeijer and Kuhne, 2014). During the last decade, around 300–400 tornadoes have been recorded annually. Approximately 10% of tornadoes have been classified at F2 or greater on the Fujita scale (Fujita, 1981).

In Europe, tornado reports are mostly based on eyewitness observations and damage surveys (Antonescu et al., 2016) in contrast to U.S., where an X-band Doppler radar network is used for real-time tornado detection (Chen and Chandrasekar, 2016). The population density may therefore exert an influence on the number of identified tornadoes (Anderson et al., 2007). Similarly, the highest tornado density across Europe is found in Belgium, the Netherlands, and in northern Germany (50 tornadoes per 10,000 km^2) (Groenemeijer and Kuhne, 2014), which are among the most densely populated regions (around 500 people/km^2, https://esa.un.org/unpd/wpp/). On the other hand, the minimum tornado density is found in sparsely populated regions such as Scandinavia and the northern part of Russia (i.e. north of 60° N) where fewer than 2 tornadoes/10000 km^2 have been observed (Groenemeijer and Kuhne, 2014). Thus, the existing climatology of tornadoes in areas with a low population density may be non-representative.

Estimates of tornado-induced forest damage can serve as an important additional source for evaluating tornado climatology in forested and sparsely populated regions. For instance, it is known that foresters have found elongated windthrows caused by tornadoes in Eastern

* Corresponding author.
E-mail address: gis@psu.ru (A. Shikhov).

http://dx.doi.org/10.1016/j.rse.2017.10.002
Received 30 December 2016; Received in revised form 17 September 2017; Accepted 5 October 2017

Europe and Siberia since the 19th century (Voznyachuk, 1954a, 1954b). The width of these windthrows varied mostly between 10 and 100 m, but sometimes reached 400 m (Voznyachuk, 1954a). The tornadoes with F1 intensity and higher are known to possibly cause significant forest disturbances, which are represented by large groups of fallen or uprooted trees and can be identified from satellite or airborne observations (Bech et al., 2009). Satellite-derived information on tornado-induced forest damage can be used to improve the climatology of tornadoes with F1 intensity and higher in low-populated forested areas.

Sayn-Wittgenstein and Wightman (1975) made the first attempt to utilise satellite images for assessing the aftermath of tornadoes in boreal forests (in Canada). They used Landsat Multi-spectral Scanner images, which had a combination of spectral (including visible and near infrared bands), spatial (60 m) and temporal (16 day) resolution. Dyer (1988) was the first to conduct detailed analysis of elongated forest cover anomalies in South America by comparing Landsat images with aerial photos and meteorological records, and reported that these anomalies were caused by tornadoes.

Further investigations showed an overall effectiveness of using satellite data for tornado damage survey and track detection (Yuan et al., 2002; Jedlovec et al., 2006; Myint et al., 2008; Molthan et al., 2014; Taszarek et al., 2016). In particular, Yuan et al. (2002) applied 23.5-m resolution images captured by the IRS-LISS-3 sensor to estimate damage characteristics from the 3 May 1999 tornado outbreak in Oklahoma (USA). They found that analysis of the change in normalised difference vegetation index (NDVI) is an effective method for detecting tornado damage (even for F1-intensity tornadoes), especially in rural areas. Myint et al. (2008) compared the accuracy of Landsat image processing techniques to detect tornado damage tracks and found that an object-based approach exhibits the highest degree of tornado damage detection accuracy. Jedlovec et al. (2006) and Molthan et al. (2014) showed that the use of near-real-time MODIS and high resolution ASTER imagery from the NASA Earth Observing System satellites can provide additional information on tornado damage tracks reported by the weather service. Damage tracks from tornadoes with F1 intensity or greater may be more clearly evident in forested areas compared with in grassland or low-forested areas. Taszarek et al. (2016) estimated an ability of mesoscale modeling to predict the formation of the 14 July 2012 tornado outbreak in Poland. Along with the radar data, aerial photography, local damage survey and damage reports in media, these authors also successfully used data from the Landsat-based Global Forest Change (GFC) project (Hansen et al., 2013) to pinpoint the exact position of the four tornado damage tracks. In general, all current studies of tornado-induced disturbances in forests have focused on the analysis of a-priori known tornadoes.

The main purpose of our study is to find previously unreported tornadoes, which imprinted their tracks in forests. We present a method that can help to supplement climatologies of F1 and stronger tornadoes in a boreal forest zone of northeast Europe (NE). Our method is based on accounting of tornado tracks in forests derived from GFC data, Landsat and high-resolution satellite images and additional supplementary data (weather stations observations, damage reports in media and reanalysis data).

We applied the method to forested regions of the NE located within 52°–67° N and 27°–60° E. The percentage of forestation varies here from 10% to 98% with the maximum located in the eastern part between 59°–64° N and 45°–60° E (Arino et al., 2008). This territory was chosen due to its substantial forestation, low population density (fewer than 10 people/km^2 for most of areas (National Atlas, 2009)), and lack of systematic information on tornado occurrences.

2. Tornado track identification in the forested area

2.1. Selection of tornado-induced forest damage

The proposed approach is based on the association of particular elongated windthrows with tornado tracks. A detailed analysis of geometrical features of forest disturbances allows accurate discrimination of their sources, including tornadoes. We identified tornado-induced forest disturbances with two steps: searching for candidates and then conducting a detailed inspection of the identified candidates.

Candidates for tornado-induced disturbances are determined based on the GFC data (Hansen et al., 2013). GFC data include information on global tree cover extent, forest loss and forest gain at a 30 m spatial resolution between 2001 and 2014 period (http://earthenginepartners.appspot.com/science-2013-global-forest). This information was obtained based on decision trees implemented on the Landsat satellite images: forest loss was defined as a stand-replacement disturbance or the complete removal of tree cover canopy at a particular Landsat pixel; the year of forest loss is determined using information about the maximum annual decline in the per cent tree cover and the maximum annual decline in the minimum growing season NDVI (Hansen et al., 2013). Year-to-year variations of forest cover had been validated with MODIS and high-resolution imageries from Google Earth (Hansen et al., 2013: Potapov et al., 2011, 2012, 2015).

In this study, we used information on forest loss from the GFC data to find elongated forest disturbances, which can be imprints of tornado tracks. The original Forest Loss Year (FLY) product of GFC data lacks information on the causes of forest losses; however, FLY provides geometrical characteristics of every disturbance. In general, all causes can be divided into four broad categories. These are man-made causes (e.g. logging), biological activity (e.g. outbreaks of insects), forest fires, and severe weather (e.g. windstorms, ice storms and tornadoes) (Baumann et al., 2014). Man-made clear-cuttings usually have a geometrically straight imprint in forests (e.g. squares, rectangles, lines), while impacts of pathogens and forest fires are referred to areas with no specific shape. Windstorms and ice storms usually cause amorphous spatial structure of forest disturbances and irregular distribution of the degree of forest damage. In turn, a tornado passing through a forest is usually characterised by an elongated geometry of the damaged area with almost complete removal of forest stands (Bech et al., 2009).

Because a tornado's path length usually exceeds a tornado path width by > 10 times (SPC data) (Schaefer and Edwards, 1999), we selected narrow and elongate areas of forest disturbances as candidates for tornado tracks, with a typical length from a few km to > 50 km and a width from 50 to 2000 m. We separated such forest disturbances from all other geometrical types based on visual interpretation. Their delineation was then performed automatically using a raster-vector transformation of their boundaries from FLY raster dataset. Fig. 1 shows an example of the GFC data implementation to identify the tornado track that occurred on 7 June 2009 in NE (Perm region, Russia). The Landsat images, obtained before and after the tornado, show the tornado-induced forest cover disturbances.

In the second step, we verified selected candidates for tornado tracks using high-resolution satellite images that are available from public map services (Google Maps, Bing Maps, Here, ESRI and Yandex.Maps). These images are derived from three main sources: DigitalGlobe (WorldView-2 satellite) imagery with spatial resolution reduced to 0.6 m; GeoEye (Ikonos satellite) imagery with spatial resolution reduced to 1 m, and SPOT-5 data with 2.5 m resolution (more details on satellite images that used in public map services can be found at: https://www.arcgis.com/home/item.html?id=10df2279f9684e4a9f6a7f08febac2a9, or: https://yandex.ru/company/technologies/satellite/). The main purpose of this verification was to obtain information about the direction of fallen trees. Indeed, windstorm-induced forest disturbances are characterised by a vector of fallen trees, which corresponds to the main wind direction of a storm (Fig. 2a). In turn, a counterclockwise rotation (infrequently clockwise) of fallen trees is the main feature of tornado-induced forest damage (Fig. 2b). Consequently, narrow and elongated forest disturbances with total canopy removal and counterclockwise-lying fallen trees were classified as tornado tracks. Additional examples of large tornado tracks in the boreal forests of European Russia are presented in Fig. 3.

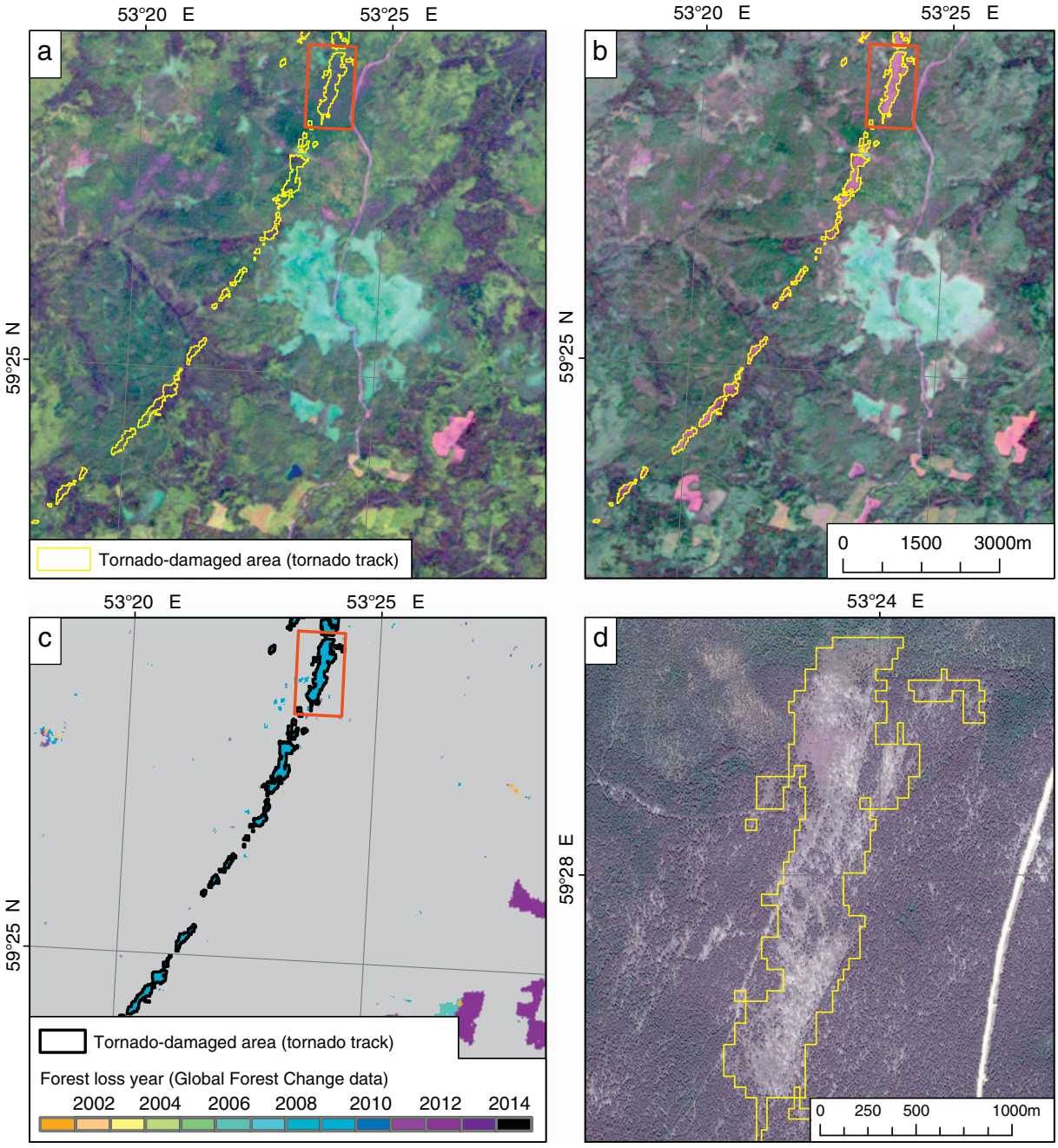

Fig. 1. Identification of a tornado track in a forested area using Landsat images and Global Forest Change (GFC) data: Landsat 5 TM images obtained on 18 Aug 2007 (a) and 8 Sep 2009 (b) before and after the tornado, forest losses by GFC map (with year disaggregation) (c), and SPOT-6 satellite image of tornado track obtained on 12 July 2014 (d). Tornado track outlined based on Forest Loss Year dataset.

Many identified tornadoes have an intermittent imprint of the tornado track (i.e. 'skipping tornadoes'). This comes from tornado intensity fluctuations or short-term lifting of the tornado from a surface (Doswell and Burgess, 1988; Godfrey and Peterson, 2017). 8–16 km (5–10 miles) is accepted as a maximum size for gaps in a continuous, but skipping tornado (Doswell and Burgess, 1988). In this paper, we used an 8-km threshold for the gap to separate one skipping tornado from two successive tornadoes.

In total, we found 135 candidates for tornado-induced forest disturbances, 110 of which were confirmed as tornado tracks based on high-resolution satellite images. 109 tornadoes in NE occurred for the 2001–2014 and one tornado occurred in 2000 (for which forest damage was erroneously attributed to 2001 by GFC).

2.2. Determination of tornado event date

The dates of forest loss are determined with a one -year accuracy in the GFC project. To determine a more precise date of a tornado event, we used additional information such as weather station observations, reanalysis data, damage reports in the media, and different satellite observations (weather radar data were not available).

First, we defined the possible time range of a given tornado event using all available Landsat Thematic Mapper (TM), Enhanced Thematic Mapper (ETM +) and Operational Land Imager (OLI) images for each tornado track. Because of excessive cloudiness in the considered regions (Chernokulsky et al., 2011), the frequency of obtaining cloudless Landsat images, and hence the accuracy of tornado date determination

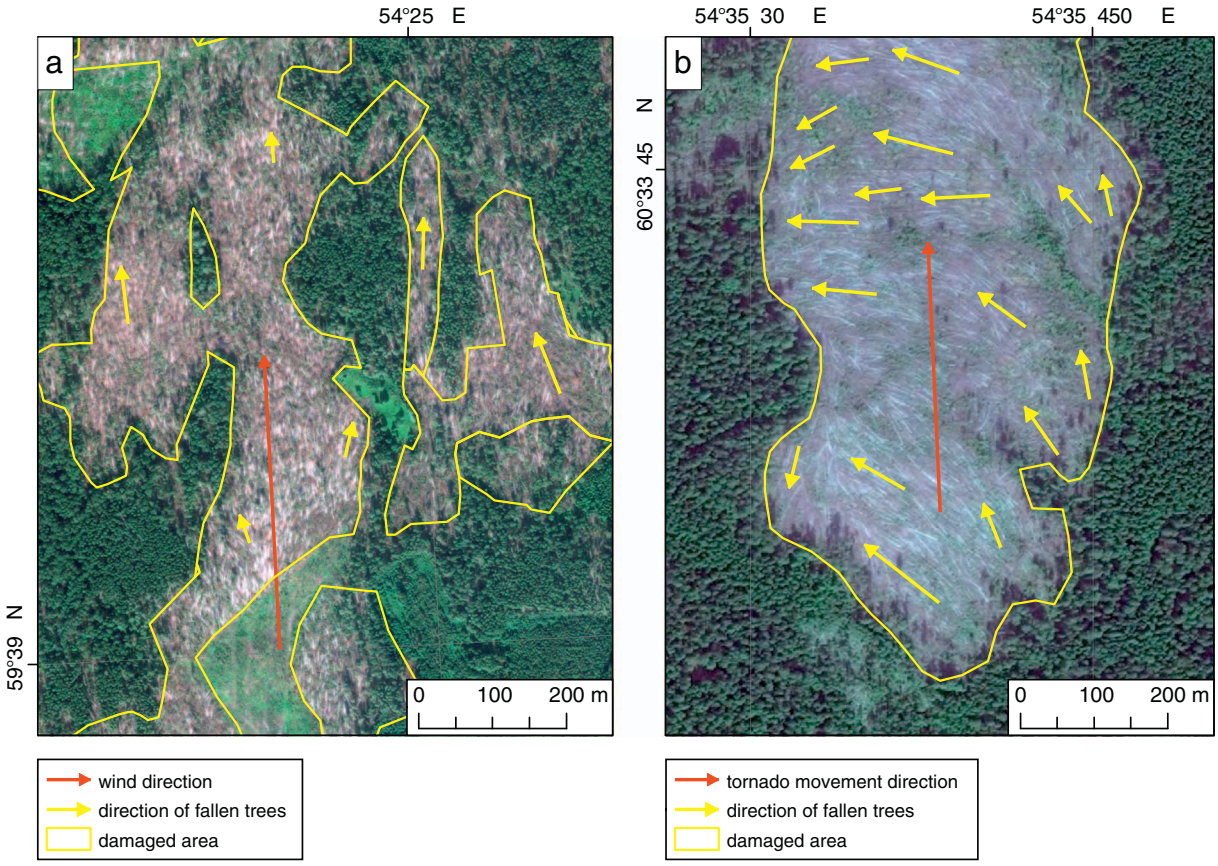

Fig. 2. Features of forest disturbances due to windstorm (a) and tornado (b) on WorldView-2 satellite images obtained 08 Aug 2012 and 14 July 2014. Red arrows indicate the direction of wind or tornado movement, yellow arrows indicate the direction of fallen trees. Damaged area is contoured with the thick yellow line. (For interpretation of the references to colour in this figure legend, the reader is referred to the web version of this article.)

by GFC data varied from one week to three months. Based on GFC validation results (Hansen et al., 2013), the year of forest disturbances was estimated correctly for 75.2% of the forest loss regions, and 96.7% of loss events that occurred within one year before or after the estimated year of disturbance. Consequently, some tornadoes may be mistakenly referred to have occurred in the following year (e.g., if they occurred in August or September). This is typical for 2003–2005 and 2008, when the frequency of obtaining Landsat data was minimal (Potapov et al., 2015). To manage this problem, winter cloudless Terra/Aqua MODIS images with 250 m spatial resolution were utilised. The year of tornado-induced forest disturbances (with a maximum width > 150 m) was specified based on a comparison of MODIS images obtained in the preceding and following winters. This was possible, because the brightness contrast between the forest canopy and snow-covered treeless area (including tornado tracks) during the winter season is significant.

We then discriminated meteorological conditions, which are favourable for tornado formation based on the NCEP Climate Forecast System Reanalysis (CFSR) data, that have high spatial (0.5°) and temporal (6 h) resolution (Saha et al., 2010). These conditions are characterised by moderate or strong convective instability (convective available potential energy (CAPE) > 1000 J/kg) (Blanchard, 1998) and large values of storm-related wind shear (storm relative helicity for lower 3 km ($SRH_{0-3\ km}$) > 250 $m^2\ s^{-2}$) (Davies-Jones et al., 1990; Doswell and Schultz, 2006). Also, a significant horizontal temperature gradient (generally, 5–12 °C/500 km), high wind speed in the middle troposphere (generally, > 20 m/s) and high moisture content (total precipitable water > 25 mm) were important. In particular, strong tornadoes (with F2 intensity and higher) in NE usually occur in cyclones, which involve maritime air masses with high moisture contents, like southern cyclones, which form over the Mediterranean or Black Sea (or passed these regions), and then move to the northeast (Snitkovskiy, 1987; Finch and Bikos, 2012). For selected days with favourable conditions for tornado formation, we compared mean wind direction in the lower and middle troposphere with tornado track vectors, which should somewhat correspond (Klemp, 1987). Thus, in some cases it was possible to obtain the date of tornado formation by matching these directions. However, this approach may give no result, when an interval between two subsequent satellite images exceeds 2–3 months. For such a long period, more than one synoptic situation that is favourable for tornado formation may occur.

Additionally, we examined weather reports from meteorological stations located near tornado tracks and information published in the mass media or social networks. In some cases, it allowed us to specify dates of a tornado occurrence. However, we should note that the weather station network is very sparse in the studied area. In this region, only one tornado event is known over the past 15 years, which was reported by an observer at a weather station, and two cases, when the tornado passed near weather stations (observers reported only severe wind gusts but not a tornado).

We were able to reliably (with accuracy of a few hours) estimate the date for 36 tornadoes. In the other 74 cases, the accuracy varied from 7 to 8 days to 3 months. The worst dating accuracy was obtained for tornadoes in 2003–2006 due to the low availability of Landsat data.

Table 1 summarises the information on datasets that were used for tornado track identification.

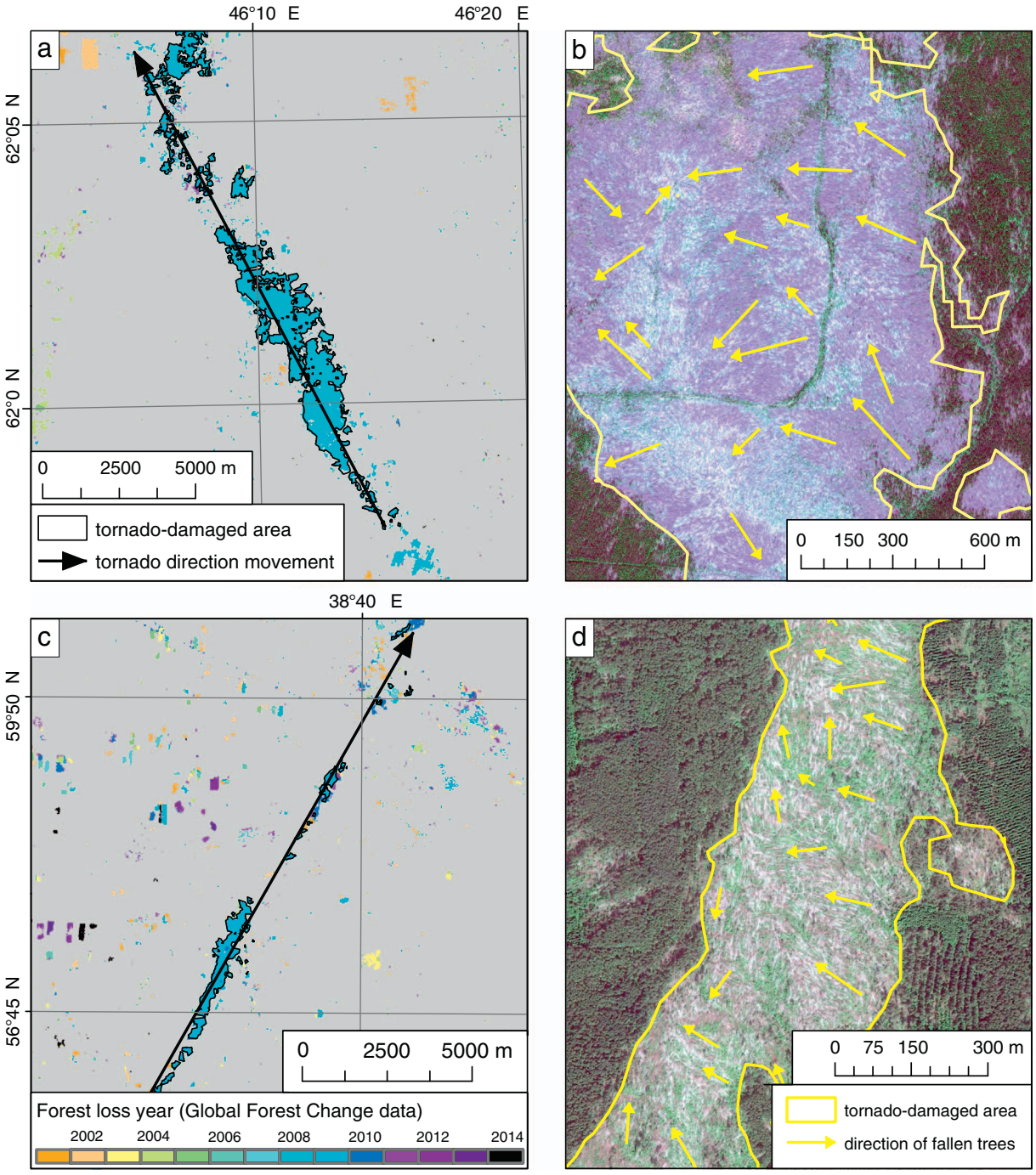

Fig. 3. Forest damage caused by tornadoes of 26 June 2008 and 03 June 2009: forest losses by Global Forest Change map (with year disaggregation) (a, c), and WorldView-2 images of tornado tracks, obtained on 27 June 2010 and 25 June 2010 (b, d). Yellow contours indicate damaged area (tornado track), black arrows show the direction of tornado motion. Red rectangles denote the position of high-resolution satellite images. (For interpretation of the references to colour in this figure legend, the reader is referred to the web version of this article.)

3. Tornado characteristics estimate

3.1. Estimate of path length and width

Geometric parameters of tornado tracks were estimated based on GFC data, and studied in detail using by high-resolution satellite images. We determined the tornado path length (L_{tp}), mean and maximum tornado path widths (WM_{tp} and WX_{tp}, respectively) and tornado-damaged area (A_{tp}) (Fig. 4).

L_{tp} was defined as a length of the central line drawn through a damaged area. It was calculated using ArcGIS and then checked manually. WM_{tp} was determined as an average width of damaged area measured by several transects perpendicular to the observed tornado path, without accounting for areas where the tornado did not touch the forest canopy (Fig. 4). Treeless regions were also not taken into account when estimating WM_{tp}. To choose the step between transects, we calculated WM_{tp} for 25 randomly selected tornado tracks with transects that sliced every 30 m (Landsat resolution, WM_{tp_30}), 100, 200, 300, 400, 500 and 1000 m. We found that the root mean square error (RMSE) does not exceed 5% of WM_{tp_30} for WM_{tp_100} and WM_{tp_200}. Thus, we choose 200 m as an optimal step between transects for the WM_{tp} calculation.

Table 1
Datasets used for tornado tracks identification.

Step of the algorithm	Used data	Data source	Spatial resolution	Temporal resolution
1. Selection of candidates for tornado-induced forest disturbances	Landsat-based GFC data (Forest Loss Year product)	University of Maryland	30 m	1 year
2. Detailed inspection of the identified forest disturbances	High resolution satellite images	Public map services (Google Maps, Bing Maps, Here, ESRI, Yandex.Maps)	0.5–2 m	1–3 years
3. Determination of tornado event date	Landsat images (TM, ETM +, OLI products)	U.S. Geological Survey	30 m	16 day
	MODIS images	U.S. National Aeronautics and Space Administration	250 m	Daily
	CFS reanalysis data	U.S. National Center for Atmosphere Prediction	0.5°	6 h
	Weather station reports	All-Russia Research Institute of Hydrometeorological Information - World Data Centre	–	3 h
	Media reports	Newspapers, Social networks	–	–

For regions with the largest transects, high-resolution images were used to manually determine WX_{tp} (except for one tornado track, which did not have high-resolution images for the region with the largest transect; its WX_{tp} was defined from GFC data). A_{tp} was calculated in ArcGIS as the sum of all forest damaged areas from FLY product, which attributed to one tornado (skipping or continuous). It is important to note that treeless land was not considered in the calculation of the damaged area. For each tornado, we also obtained positions (latitude and longitude) of the start, centre and end of its track, direction of movement and sense of rotation (in the presence of high-resolution images of damaged area).

To evaluate the accuracy of GFC-obtained tornado track geometrical parameter estimates, we compared those automatically identified by GFC data with those that were manually vectorised from very high-resolution satellite images. A similar approach was previously used to assess the limitations of automated detection of wind-induced forest disturbances based on Landsat images (Koroleva and Ershov, 2012). They showed that a reliable estimate (within 15% accuracy) of a given damaged area using Landsat images is possible if the area exceeds 2.6 ha.

We randomly selected 25 tornado tracks (with a somewhat uniform distribution of L_{tp} and WM_{tp}) and compared their geometrical

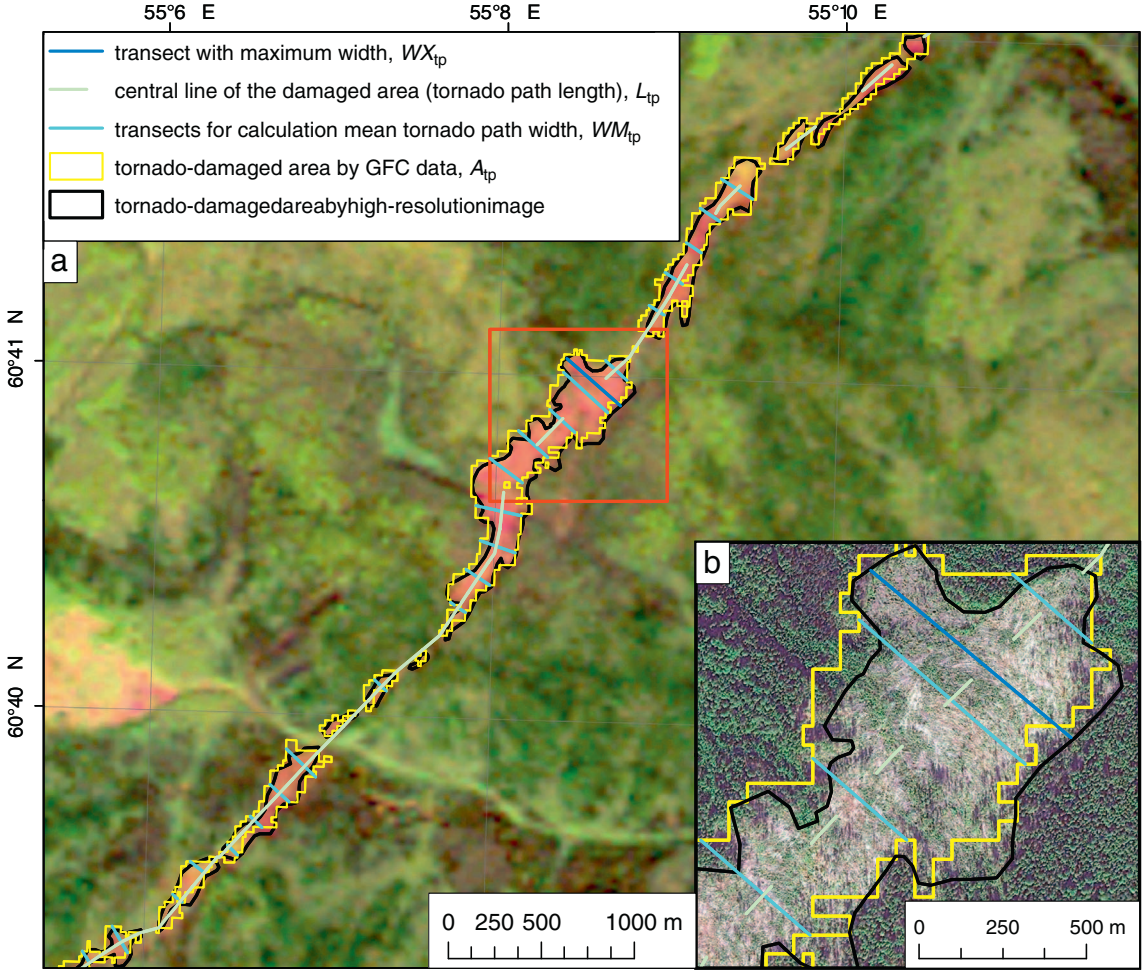

Fig. 4. Scheme for the measurement of geometric parameters of tornado tracks in forests based on Landsat-5 TM images, obtained on 8 Sep 2009 (a) (for L_{tp}, WM_{tp} and A_{tp}) and WorldView-2 satellite image obtained on 26 Aug 2012 (b) (for WX_{tp}) (see text for more details).

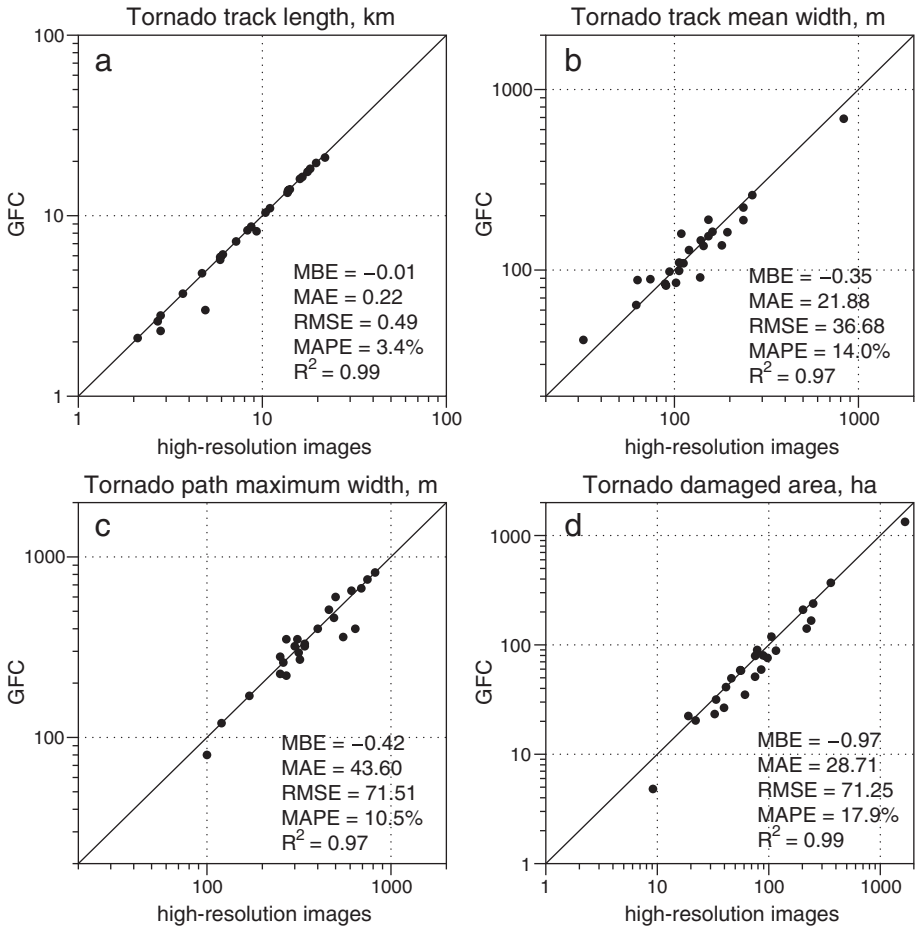

Fig. 5. Comparison of tornado path length (a), maximum width (b) and tornado-damaged forested area (c) estimated by Global Forest Change and by high-resolution satellite images. The mean bias error (MBE), mean absolute error (MAE), root mean square error (RMSE), mean absolute percent error (MAPE), and determination coefficient (R^2) are shown. Note the logarithmic scales for all figures.

characteristics obtained from GFC data with those from high-resolution images (Fig. 5). We found a better agreement between different data for L_{tp} than for WM_{tp}, WX_{tp} and A_{tp}. GFC data tend to slightly underestimate L_{tp} of tornadoes with a short path (< 10 km). For WM_{tp} and WX_{tp}, the difference between data is larger (GFC data both underestimate and overestimate WM_{tp} and WX_{tp} that results in close-to-zero mean biases). Thus, for 11 out of 25 tornadoes the difference between WX_{tp} values obtained from GFC and high-resolution images exceeds 10% of the magnitude of WX_{tp} (up to an additional 30% for some tornadoes). For this reason, we aimed to obtain WX_{tp} for all cases from high-resolution images.

GFC data generally tend to underestimate A_{tp} (16 cases out of 25 are underestimated). The mean absolute per cent error for A_{tp} (17.9%) is higher than those for L_{tp} and WX_{tp} (for weak tornadoes with a low impact, the difference of A_{tp} between different data is up to 30%). As a result, estimates for WM_{tp}, WX_{tp} and A_{tp} are biased and should be accompanied by the use of high-resolution images. However, in our analysis only WX_{tp} were specified using high-resolution images. Systematic bias for WM_{tp} and A_{tp} (around 10 and 20% respectively) should be kept in mind. GFC data can be used for an accurate estimation of L_{tp}; however, when a tornado starts or terminates outside out of forest boundaries (or becomes too weak to make any damage), L_{tp} tends to be underestimated.

3.2. Tornado intensity

For completing tornado climatology, it is of particular interest to evaluate the intensity of the detected tornadoes. For instance, it is important for economic purpose (e.g. infrastructure of building industry) to estimate the risk of strong tornado formation. However, a determination of tornado intensity is challenging due to the absence of necessary supplementary information. In particular, satellite images do not provide information on the type of tree' damage; it is therefore unclear if they were only uprooted, snapped or debarked. Lack of detailed information on the orientation and degree of every fallen tree damage, species composition and terrain features, in addition to a lack of exact date for some tornadoes, does not allow reconstruction of the near-surface wind field in the fashion of studies based on aerial photography data and comprehensive tree models (Holland et al., 2006; Beck and Dotzek, 2010; Karstens et al., 2013) or simplified coupled wind and tree resistance models (Godfrey and Peterson, 2017).

Another approach to estimate tornado intensity is to relate it with tornado path characteristics. Thus, Pisnichenko (1994) approximated the Fujita-scale (F-scale) intensity (FI) of a tornado by its path width using a power law based on tornado reports for the fUSSR region (dataset from Snitkovskiy, 1987). This dataset contains information about 248 tornadoes; however, only 77 of them are accompanied with the estimate of tornado width (55 of them have estimates of both tornado width and length). Because of the small number of cases (and consequentially weak statistical significance), we decided to rely on the results of Brooks (2004), who applied a Weibull distribution to model tornado path lengths and widths for different F-scale ratings and found a good match of the modelled values with observations in North America (> 40,000 cases from the SPC data). However, Brooks mentioned that an exact F-scale rating cannot be restored in that manner. As a consequence, we used the Weibull distribution parameters obtained by Brooks (2004) to evaluate the probability of a minimal tornado FI. In order to do so, we calculated the probability of exceedance of each FI rating for each path length (and maximum width). For simplification, tornado path lengths and widths are considered as independent values;

the probability of a minimum tornado FI for a certain tornado path length and width (P_{LW}) is calculated as the probability of the union of two independent events (only-length-based and only-width-based probabilities of minimum FI, P_L and P_W respectively) where $P_{LW} = P_L + P_W - P_L P_W$.

There may be concerns regarding how appropriate it is to apply statistics based on U.S. tornadoes to NE region. Groenemeijer and Kuhne (2014) showed a general consistency between U.S. and European tornadoes in terms of their path widths and lengths. They showed that strong tornadoes (F2 and higher) in Europe tend to be a bit shorter than in the U.S., while weak tornadoes (F0, F1) are a bit longer. The maximum path widths of European tornadoes are smaller than those from the U.S.; however, it may be underestimated because most European cases have not been verified as carefully as in U.S. cases (Groenemeijer and Kuhne, 2014). Consequently, Weibull-based estimated intensities may be slightly underestimates when applied to European tornadoes. Because we focus on the exceedance of the FI rating, this underestimation leads to more robust evaluations of the minimum FI. However, one should keep in mind that the presented tornado intensity estimates are given in probabilistic terms and should be treated with caution when compared with well-developed ground survey-based estimates. Moreover, we can estimate only minimum intensity, rather than the actual one. Fig. 6 presents the 0.75 and 0.9 estimated probabilities (P_{LW}) of exceedance of different FI (shown by lines). Grey symbols correspond to investigated tornadoes that were identified by forest disturbances. It can be seen that four tornadoes from our database have intensities that exceed F2 level with a 0.9 probability. Colour symbols stand for cases of tornadoes over the European part of fUSSR, for which paths and widths were defined: 55 cases from Snitkovskiy (1987); 14 cases from (Recommendation on…, 2002) and 13 cases from ESWD data (Groenemeijer and Kuhne, 2014) (82 tornadoes in total). In general, the intensities of observed tornadoes fit well to the calculated ones. Thus, from the 74 cases in the area with F1 from a Weibull-based estimated intensity (with $P_{LW} \geq 0.9$), only three tornadoes have F0 intensity (3/74 ≈ 0.04). From 26 cases in the area with F2 minima from Weibull-based estimated intensity (with $P_{LW} \geq 0.9$), only four have F1 intensity (4/26 ≈ 0.15). Only two observed tornadoes have a large enough path length and/or width to be in the area with F3 minimal Weibull-based estimated intensity (with $P_{LW} \geq 0.9$); one of them has F3 intensity and another has F4.

4. Tornado climatology in forested regions of northeast Europe in 2000–2014

Based on the methodology described in Section 2, our study found plausible estimates of 110 tornadoes in the forested regions of NE in 2000–2014 years; 105 of these were previously unreported and discovered for the first time. 64 tornadoes (58.1% of all tornadoes investigated) have F1, 42 tornadoes (38.2%) have F2, and 4 tornadoes (3.6%) have F3 minimum estimated intensities (with $P_{LW} \geq 0.9$) (see Section 3 for more details). Taking into account that the presented method allows an estimation of only the minimum intensity, the obtained distribution is in reasonable agreement with that from the ESWD data. Thus, among the 3013 tornado events in ESWD with intensities greater that F0, 1692 (56.2%) tornadoes have an F1 rating, 984 (32.6%) have F2 and 337 (11.2%) have F3 and higher (Groenemeijer and Kuhne, 2014).

4.1. Spatial distribution of tornadoes

The spatial distribution of the studied tornadoes is shown in Fig. 7 with an indication of their intensities. The density of tornado tracks was calculated based on the kernel density method (Silverman, 1986) using ArcGIS 10 software. In our approach, the spatial distribution of tornado tracks was associated not only with tornado frequency but also with the percentage of forestation, which was used as a weighting coefficient. The percentage of forestation was estimated using a GlobCover-2009 vegetation map (Arino et al., 2008). The tornado density weighted by the percentage of forested area (D_t), was calculated by dividing the original tornado density (obtained based on the kernel density method implemented to identify tornado tracks (D_{to})), by the ratio of forest-covered area (f_c): $D_t = D_{to} / f_c$. Thus, for regions with $f_c = 0.8$ (80%) and $D_{to} = 3$ tornadoes per 10,000 km^{-2}, D_t will be equal to 3.75 tornadoes per 10,000 km^{-2}.

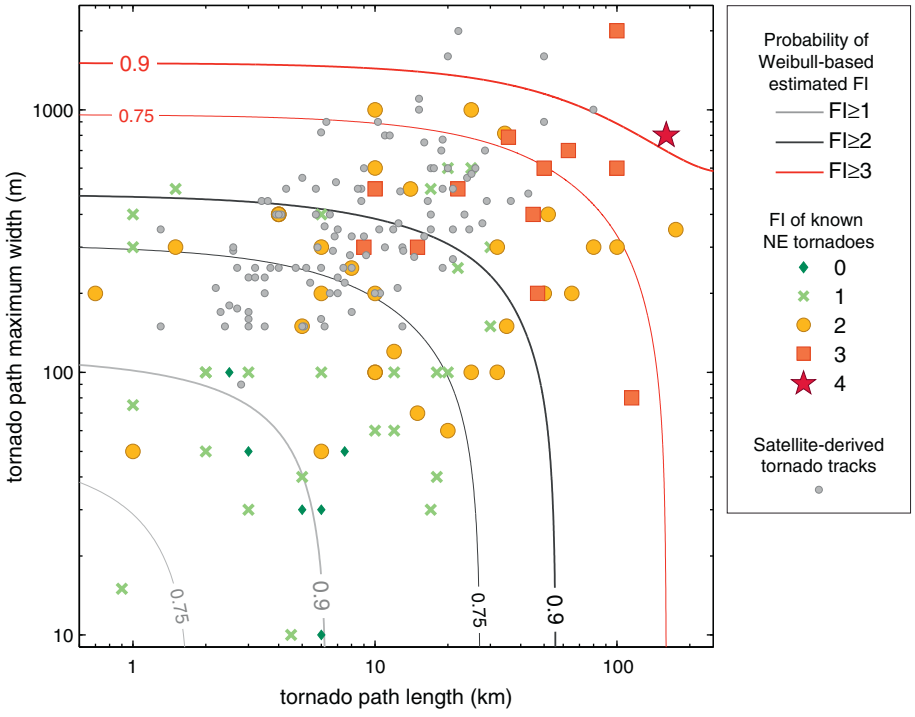

Fig. 6. Estimated probabilities of exceedance for different F-scale intensities (grey lines for F1, black lines for F2, red lines F3; thin lines for 0.75 probability and thick lines for 0.9 probability) calculated based on Weibull distribution parameters (Brooks, 2004). Known tornado events (in the European part of fUSSR) are shown by colour symbols (different symbols for different Fujita intensity). Investigated satellite-derived tornado events are shown by grey symbols. Note the logarithmic scales. (For interpretation of the references to colour in this figure legend, the reader is referred to the web version of this article.)

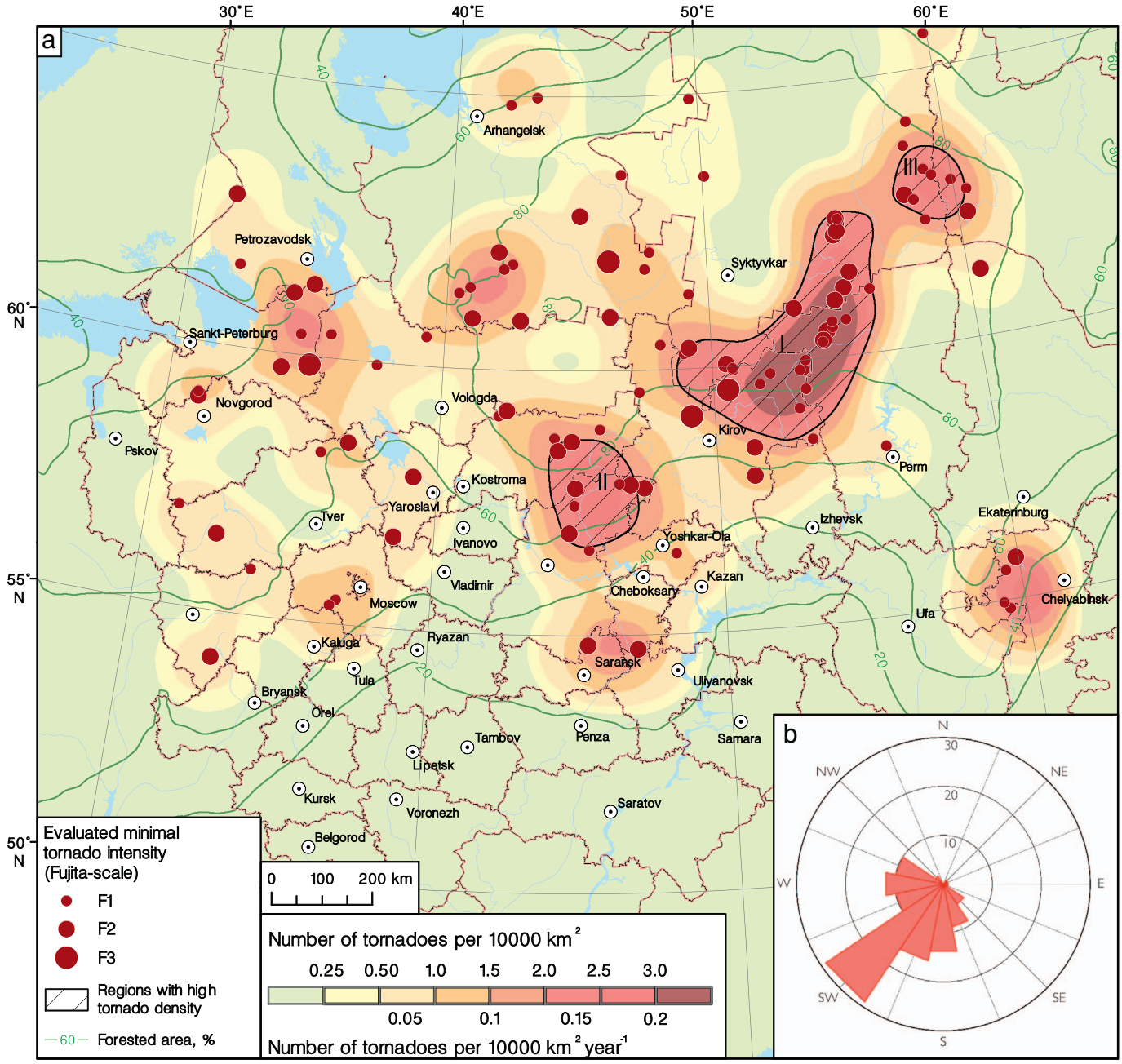

Fig. 7. Spatial distribution (a) of tornado tracks identified by satellite data in forested regions of northeast Europe in 2000–2014, with probabilistic estimates of Fujita intensity exceedance (shown by symbol colour and size) and tornado density weighted by the percentage of forested area (shown by shaded areas); tornado movement direction (b) (the direction from which it originates, presented in 16 rhumbs).

Three areas with a comparatively high tornado density (D_t) can be highlighted:

1) 28 tornado tracks (including 5 tracks which the maximum path width exceeds 500 m, 12 tracks with F2 minimum estimated intensity) were identified within the eastern part of NE (located between 59°–62° N and 49°–55° E). The forest cover percent (f_c) here is > 90%, which allows identification of almost all intense tornadoes; D_t is up to 3.8 tornadoes per 10,000 km^2.
2) 11 tornadoes were identified in the Volga region (56°–59°N and 44°–48°E, f_c ~70%); D_t is around 2.9 tornadoes per 10,000 km^2.
3) 11 tornadoes were found in the Northern Urals (61°–64°N, 58°–61°E, f_c > 90%); D_t reaches 2.6 tornadoes per 10,000 km^2. Note, that 6 out of 11 cases occurred here during the 23 June 2007 tornado outbreak.

These three areas form somewhat of a 'forest tornado alley' that stretches from southwest to northeast.

Interestingly, the direction from southwest to northeast is the most common for tornado movement (Fig. 6b) (26.5% of all cases, if presented in 16 rhumbs; 39.1% if presented in eight rhumbs). Directions from west to east and from south to north are also common. This is in general agreement with previously reported estimates. Snitkovskiy (1987) presented tornado direction movement in eight rhumbs and found that most of the tornadoes in NE move from southwest to northeast in a proportion even higher (73% of all tornadoes) than those found here. The prevailing direction from southwest to northeast is determined by propagation in the same direction of active cyclones with warm moist air, which determine the most favourable conditions for tornado formation in NE) (Snitkovskiy, 1987).

More than a half of the identified tornado tracks (58 out of 110) are

located north of 60° N. Lack of latitudinal mountain chains in NE gives the possibility for tropical air masses to freely spread northward to the Arctic coast and interact with cold air masses. Thus, significant temperature gradients are often formed in northern regions of NE, which yield convectively unstable conditions (Kurgansky et al., 2013). Voznyachuk (1954a) was the first to discuss the possibility of tornado formation in the northern part of NE and provided historical data on several cases of northern tornadoes in Europe and Russia (with latitudes up to 58°–61° N). Subsequent databases (Snitkovskiy, 1987; Groenemeijer and Kuhne, 2014) contain further information on some northern tornadoes. However, these data are based on eyewitness-obtained information, which unequivocally leads to tornado number underestimation in regions with low population density such as northern regions of NE. Our method is independent of population density and observational networks and provides unique information on dozens of northern tornadoes. According to our data, the northern boundary of the tornado distribution in NE is located close to the Arctic Circle. The northernmost tornado was observed at 65.61° N, 59.81° E in the territory of the Komi Republic in August 2011.

4.2. Interannual and monthly variability of tornadoes

Among the 110 identified tornadoes, the accuracy varied from a few hours (for 36 tornadoes) to three months (four cases). We were able to identify the year of all tornadoes (note, that one occurred in 2000; however, GFC data span from 2001 to 2014). Fig. 8a presents the interannual variability of tornadoes. The largest number of tornadoes was noted in 2009 (24 tornadoes). In 2004 and 2007, a comparatively high number of tornadoes were found as well. However, a maximum of tornadoes occurring in 2006, as reported by Groenemeijer and Kuhne (2014), was not revealed in forested regions of NE. The interannual distribution of strong tornadoes (FI ≥ 2) has a maximum in 2009 when 11 strong tornadoes had formed. In other years, the number of identified strong tornadoes varied from zero to five (Fig. 8a). Two tornadoes with FI ≥ 3 occurred in 2012, and one such tornado happened in 2012 and 2013. No tornadoes were identified in 2014.

Monthly variability of tornadoes is shown in Fig. 8b (note, that only 79 tornadoes with a maximum dating accuracy of two weeks taken into account). The earliest event occurred on 12 May, while the latest event dates are from the beginning of September. The maximum tornado frequency is observed in June, when 44 events were recorded (Fig. 8a, b). The monthly distribution of strong tornadoes also has a maximum in June. However, strong tornadoes may form in May, July and August as well. Our findings are in agreement with previous studies, that also showed the maximum of tornadoes over NE in June (Snitkovskiy, 1987; Groenemeijer and Kuhne, 2014). On the one hand, the high frequency of tornadoes in June may be associated with greater baroclinicity in the early summer (Lehmann et al., 2014), while low gradient pressure fields and blocking anticyclones, which are unfavourable for tornado formation, are more typical in mid-summer (Timazhev, 2016). On the other hand, in May and June, the maximum local temperature gradients between Arctic and tropical air masses are observed in the considered regions (based on the analysis of ERA-Interim data for the northern part of NE (55°–65° N, 30°–60° E), frequency of the temperature gradient > 0.1 K km^{-1} is close to 0.006 in May, 0.005 in June and only 0.002 in August). In addition to the temperature and pressure gradient, tornado formation also requires the advection of air masses with relatively high temperatures and moisture contents that lead to substantial convective instability, which is unusual for NE in May (e.g. CAPE over NE has its maximum in July). Thereby, the maximum of tornado frequency is observed later than the maximum of local temperature gradients. Additional studies are required to robustly establish the major causes of monthly and interannual variability of the number of tornadoes in NE.

4.3. Tornado path lengths and widths

More than a half of all identified tornadoes (64 out of 111) have a path length (L_{tp}) < 10 km (Fig. 9a). Such magnitudes of L_{tp} are typical for F1 or F2 tornadoes, according to the observations in Europe and the U.S. (Groenemeijer and Kuhne, 2014). According to Snitkovskiy (1987), the average L_{tp} in the fUSSR is notably larger (about 25 km and varies from 1 to 160 km). Our method slightly underestimates L_{tp} (see Section 3.1 for details); however, we suspect that the longest tornado paths in the Snitkovsky database may be overestimated. Based on satellite data, we found five tornadoes with L_{tp} > 30 km. The longest L_{tp} reaches 80 km, (belonging to the tornado that occurred on the night of 8 August 2012 and passed through Leningrad and Vologda regions), while the shortest L_{tp} is 1.3 km.

Most tornado tracks haves WX_{tp} values around 200–300 m (30 tornadoes), and WM_{tp} is close to 100–200 m (52) (Fig. 9b). Snitkovskiy (1987) showed similar estimates for WM_{tp} (about 160 m). In Europe and the U.S., such path width is typical for F1 and F2 tornadoes (Groenemeijer and Kuhne, 2014). For some cases, we found WX_{tp} > 1000 m. A tornado that occurred on 26 June 2008 and passed through the south of the Arkhangelsk region wasthe largest WX_{tp} (up to 2000 m). The smallest WM_{tp} had 60 m. Spatial resolution of GFC data (30 m) does not allow identification of tornadoes with smaller path widths.

Tornado-damaged area, A_{tp}, varies over a wide range, from 4 to 1470 ha for different tornadoes (Fig. 9c); however, more than half of the investigated tornadoes (68) have A_{tp} < 100 ha. The largest A_{tp} was caused by a tornado that occurred on 17 June 2013 in the north of the Kirov region (1493 ha). The total damage of tornadoes to forests in NE for 15 years (i.e. sum of all A_{tp} in NE over 15 years) was 17,200 ha, which is comparatively low compared with windstorm-induced or fire-

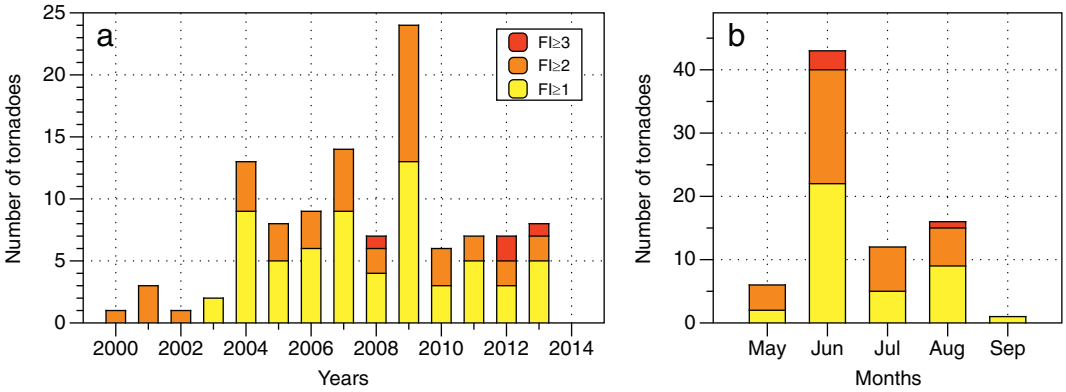

Fig. 8. Inter-annual variability (a) and monthly distribution (b) of tornadoes with the probabilistic estimates of Fujita intensity exceedance. Tornadoes with uncertain dates (i.e. uncertainties greater than two weeks) are not included in Panel b.

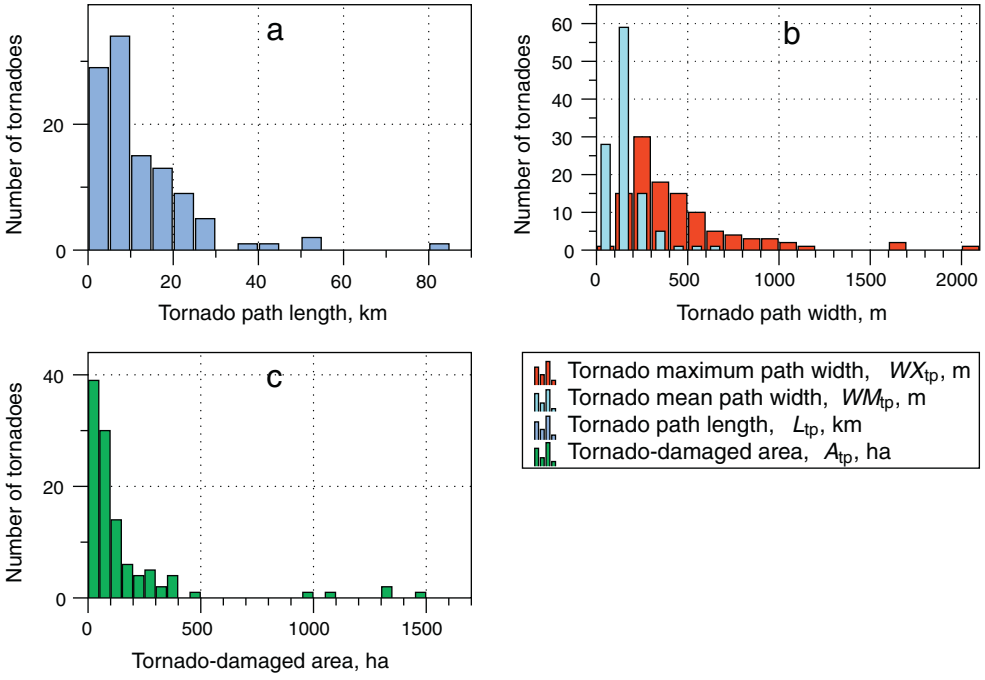

Fig. 9. Distributions of geometrical parameters of tornadoes: path length (a), mean and maximum path width (b), and tornado-damaged area (c).

related disturbances (e.g., the forest damage caused by a single severe windstorm observed on 27 June 2010 in the Yaroslavl and Vologda regions exceeded 30,000 ha). A_{tp} depends on both L_{tp} and WM_{tp} (WX_{tp}). The Pearson correlation coefficient (R) between A_{tp} and L_{tp} is 0.76, and between A_{tp} and WM_{tp} (WX_{tp}) is 0.83 (0.81) (all coefficients are statistically significant at a 0.05 level). Moreover, we found, that L_{tp} and WM_{tp} (WX_{tp}) correlate statistically significantly (at a 0.05 level) with each other (R = 0.45 (0.52)).

4.4. Tornado outbreaks and 10 most severe tornadoes

Table 2 summarises information on the ten tornadoes with the highest L_{tp} and WX_{tp} and estimated minimum F2 or F3 intensities. It is important to note, that seven tornadoes occurred in June, which is the most favourable month for strong tornadoes in NE. Some tornadoes have path lengths and widths similar to characteristics of the catastrophic 1984 Ivanovo tornado (the most violent historical tornado in NE) that had F4 intensity (Vasil'ev et al., 1985).

For seven tornadoes with known date, a more detailed analysis of atmospheric conditions was performed. These tornadoes were formed in warm sectors of cyclones that came from the southern seas (cases #1, #3, #4, and #5; for cases #3 and #5, cyclones regenerated over the Middle Volga region) or from the Atlantic Ocean (#8, #9 and #10). All of these events (except #3) are characterised by a relatively high wind speed in the middle troposphere (up to 30 m/s at 500 hPa); air masses in a warm sector had a high temperature (14–18 °C at 850 hPa isobaric level) and high moisture content (total precipitable water is 30–50 mm). Convective indices CAPE, SWEAT (Severe Weather Threat Index), SRH_{0-3km} and EHI (Energy Helicity Index) reached the critical values for most cases (Doswell and Schultz, 2006) (CAPE > 1000 J kg^{-1}, SWEAT > 300, $SRH_{0-3\ km}$ > 300 m^2 s^{-2}, EHI > 1).

Table 2
Ten tornadoes with the highest path lengths and widths. Instability indices were estimated by CFSR data (maximum values within a 300 km radius from tornado formation).

#	Date (UTC)	Coordinates (start)	Coordinates (end)	Path length, km	Maximum path width, m	Damaged area, ha	Minimum. FI (P > 0.9)	Maximum instability indices values (CAPE, J kg^{-1}/SWEAT/$SRH_{0-3\ km}$, m^2 s^{-2}/EHI)
1	25 Jul 2000	56.396° N 32.612° E	56.558° N 32.336° E	26	600	124	F2	2250/300/400/0.5
2	Aug 2004	61.244° N 34.593° E	61.428° N 35.215° E	43	480	473	F2	–
3	26 Jun 2008	61.935° N 46.282° E	62.114° N 46.125° E	22	2000	1336	F3	1200/ < 240/410/1.2
4	3 Jun 2009	56.686° N 38.523° E	56.88° N 38.731° E	25	570	309	F2	1800/400/540/2.6
5	7 Jun 2009	60.196° N 54.044° E	60.587° N 54.485° E	50	900	1095	F2	2000/400/290/2.7
6	Jun 2009	62.213° N 55.091° E	62.524° N 55.277° E	36.4	450	141	F2	–
7	Jun 2012	59.071° N 49.007° E	59.171° N 49.294° E	20	1600	996	F3	–
8	7 Aug 2012	59.81° N 35.03° E	60.177° N 35.415° E	80	1000	1343	F3	1200/350/560/1.1
9	17 Jun 2013	59.57° N 50.382° E	59.627° N 51.273° E	50	1600	1494	F3	No CFSR data
10	18 Jun 2013	62.747° N 57.842° E	62.907° N 58.27° E	29	450	353	F2	1200/400/380/1.8

Table 3
Characteristics of tornado outbreaks. Instability indices were estimated by CFSR data (maximum values within a 300 km radius from tornado formation).

#	Date	Coordinates (start)	Coordinates (end)	Number of tornadoes	Largest tornado path length and width (km)	Total damaged area, ha	Minimum FI (P > 0.9) of the strongest tornado in outbreak	Maximum instability indices values (CAPE, J kg^{-1}/SWEAT/ $SRH_{0-3\ km}$, $m^2\ s^{-2}$/EHI)
1	Aug 2001	58.481° N 44.217° E	58.748° N 44.992° E	2	19/0.77	514	F2	–
2	Aug 2004	61.11° N. 34.11° E	61.48° N 35.22° E	2	43/0.48	577	F2	–
3	Aug 2004	64.83° N 42.13° E	65.0° N 43.42° E	2	13.1/0.29	100	F1	–
4	12 May 2007	54.81° N 45.30° E	54.72° N 47.03° E	2	15.2/1.1	293	F2	1400/420/440/0.8
5	23 Jun 2007	61.22° N 60.47° E	64.14° N 58.47° E	6	11.9/0.8	660	F2	3750/450/450/3.9
6	26 Jun 2008	60.94° N 46.25° E	61.11° N 46.12° E	2 (3)	22.1/2.0	1457	F3	1200/240/410/1.2
7	07 Jun 2009	59.39° N 53.31° E	61.61° N 55.49° E	9	50/0.9	2404	F2	2000/400/290/2.7
8	June 2009	61.19° N 55.0° E	62.62° N 55.25° E	5	36.4/0.5	595	F2	–
9	12 June 2010	57.93° N 39.05° E	56.92° N 44.83° E	3	21/0.7	490	F2	2000/450/420/2.4
10	07 Aug 2012	59.56° N 34.69° E	60.17° N 35.41° E	2	80/1.0	1583	F3	1200/350/560/1.1
11	24 May 2013	55.36° N 36.61° E	55.49° N 36.87° E	2	4.1/0.4	92	F2	3500/340/190/2.3
12	31 Jul 2013	54.81° N 59.47° E	54.97° N 59.26° E	2	9.2/0.28	75	F1	2000/350/450/0.9

12 tornado outbreaks (≥ 2 tornadoes per day) were identified (Table 3). The paths of tornadoes during six tornado outbreaks, including strong tornadoes with estimated intensity ≥ F2 (P > 0.9) are shown in Fig. 10. In most cases, tornadoes occurred successively one after another, and are likely associated with the same mesoscale convective system (MCS) (Fig. 10a–c). There are also cases of quasi-parallel tornado movement, when there were two (or more) MCSs (Fig. 10e, f). We found one case with several so called 'satellite' tornadoes (Fig. 10d). Almost half of the outbreaks (5) occurred in June (Table 3). Four tornado outbreaks were happened in August. In addition to strong tornadoes (Table 2), most of outbreaks (six out of eight with a specified date) were associated with an advection of moist warm air from southern seas or the Atlantic Ocean with an active cyclone and accompanied with the critical values of convective indices (CAPE > 1000 J kg^{-1}, SWEAT > 300, $SRH_{0-3\ km}$ > 300 $m^2\ s^{-2}$, EHI > 1).

5. Discussion: primary limitations of the proposed method

The presented method aims to identify previously unreported tornadoes in boreal forests and is applicable for supplement tornado climatology in those regions. It has several apparent limitations that are discussed in this section.

With this method, it is only possible to restore information about F1 and stronger tornadoes, which have considerable impacts on forests. On the one hand, these tornadoes should be strong enough to fell trees; on the other hand, the linear size of tornado tracks should be distinguishable from the satellite data. The spatial resolution of the GFC data and Landsat images is 30 m; thus, we can confidently identify tornado tracks with a maximum width > 60–80 m. According to Snitkovskiy (1987) and ESWD data (Groenemeijer and Kuhne, 2014), 49% (44%) of those tornadoes in Northern Eurasia (Europe), whose path widths were determined have maximum paths < 100 m. Most of these tornadoes had low intensity (F0 and F1). Thus, the proposed method may miss about 40–50% of tornadoes with low intensity (F0 or F1), but is capable for identifying the more intense tornadoes.

The method cannot be used properly in low-forested regions (with forest coverage < 50%). It is possible to overlook tornado tracks when a tornado passed through areas of intensive timber harvesting or agricultural lands. For example, according to the GFC data it is difficult to identify the track of 29 August 2014 severe tornado, which was observed near Yanaul (Fig. 11) (Chernokulsky et al., 2015). The forested area in this region is about 20%, and the total area of the tornado-induced forest disturbance was 143 ha; however, it is impossible to associate the tornado-induced forest damage with the tornado passing. Some other factors may also influence the obtained results. For instance, forest fires can pass through tornado tracks and mask a tornado passing.

The proposed method allows determination of tornado characteristics with some limitations. Thus, both path length and width may be underestimated when restored with GFC data (see Section 3.1 for more details). Tornado intensity can be evaluated only indirectly and presented in probability terms. The date of tornado formation can be obtained for some tornadoes with accuracies of less than one month.

Landsat data features should also be kept in mind. For instance, a Scan Line Corrector (SLC-off) failure in Landsat-7 ETM + data can influence the identification of tornado tracks especially in low-forested regions. There was relatively low Landsat image availability between 2003 and 2005, and also in 2008, when only Landsat − 7 data were available. As a result, the frequency of obtaining cloudless images was rather low (one image per 3–6 months) to properly estimate tornado dates. It should also be mentioned that high-resolution image sources have matured significantly since the early 2000s. As a result, the appearance of new high-resolution data may, in theory, slightly skew the results of tornado track identification towards later years. However, due to the relatively slow process of natural reforestation in boreal forests (Kramer et al., 2014), the tornado-induced forest disturbances are successfully identified by high-resolution images within ten years after a tornado passing.

The approach presented here requires expert' verification at almost all stages; the number of variables limits the possibility of automation of the method. First, many identified tornadoes have an intermittent imprint in a forest because of intensity fluctuations, short-term lifting from a surface, or damaged forest areas that intersect with clear cutting and burned areas. Second, the year of forest cover disturbance is estimated with 25% error in the GFC data. As a result, one tornado track can be erroneously divided into different years. Finally, all identified

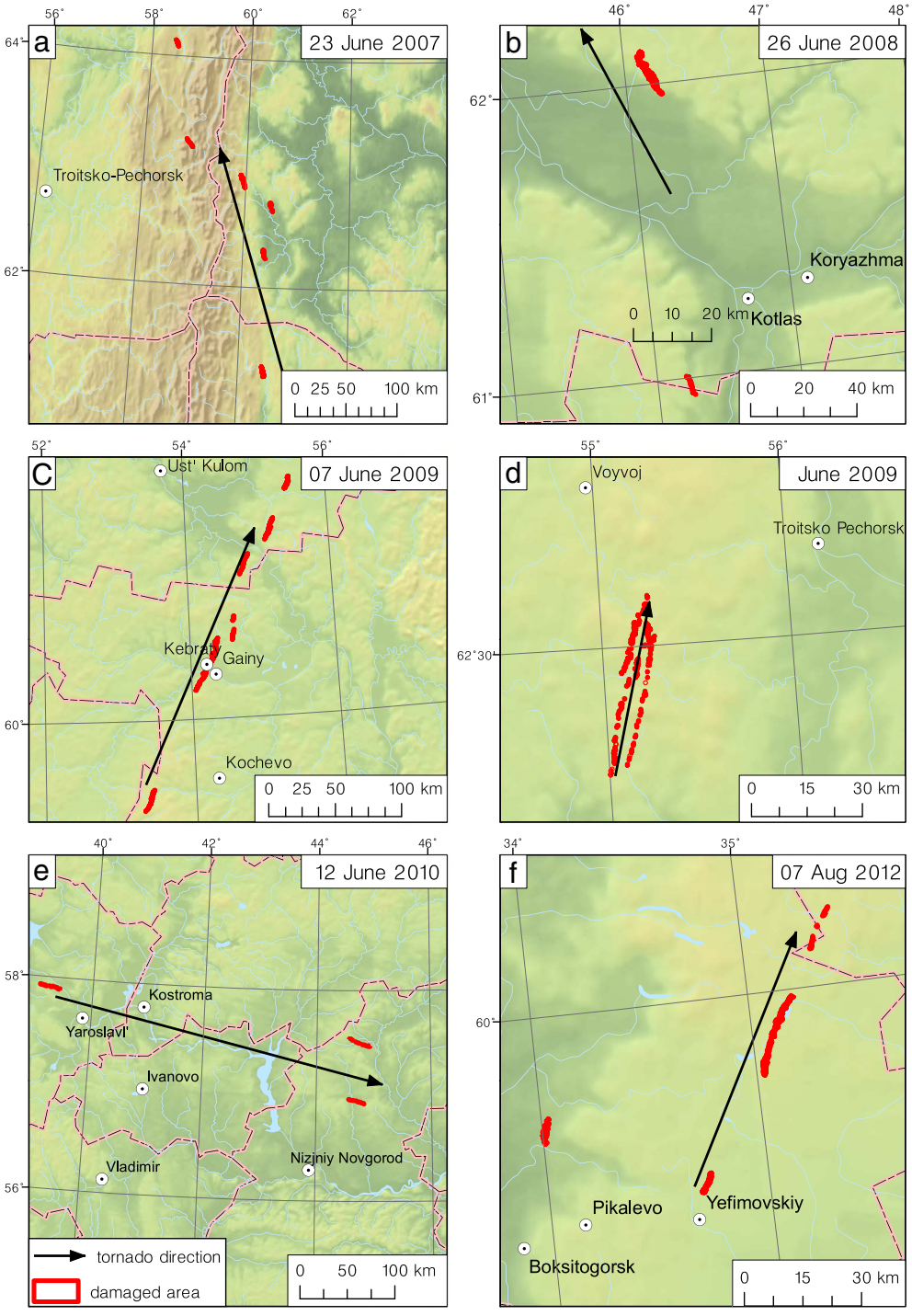

Fig. 10. Major tornado outbreaks in forested regions of northeast Europe in 2000–2014.

tornado tracks must be verified by high-resolution satellite images.

Despite all the mentioned issues, the proposed approach allows a new piece of information about previously unreported tornadoes in low-populated forested regions to be obtained, and the main characteristics of these tornadoes to be evaluated, albeit with some limitations.

6. Conclusion

We propose a novel method for tornado track identification. The method is based on the use of GFC data for searching for candidates (narrow elongated forest disturbances) that are subsequently verified with satellite images with high spatial resolution (0.5–2 m) for specifying a tornadic cause of forest disturbances. Satellite data are used for determining tornado path length and maximum and mean width. Additional information is involved to estimate the date of the tornado occurrence. Based on a Weibull distribution, probabilistic estimates of minimum tornado intensity (F-scale) are obtained depending on tornado path lengths and widths. This method allows robust identification of tornadoes with a path width that exceeds 60 m in forested regions with > 50% coverage. The presented method has been applied to NE, and is capable to complement tornado climatology in any forested region worldwide where tornadoes may form.

Based on the proposed method, 110 tornado tracks were found in forested low-populated regions of NE in 2000–2014, 105 of which were previously unknown and are subsequently reported here for the first

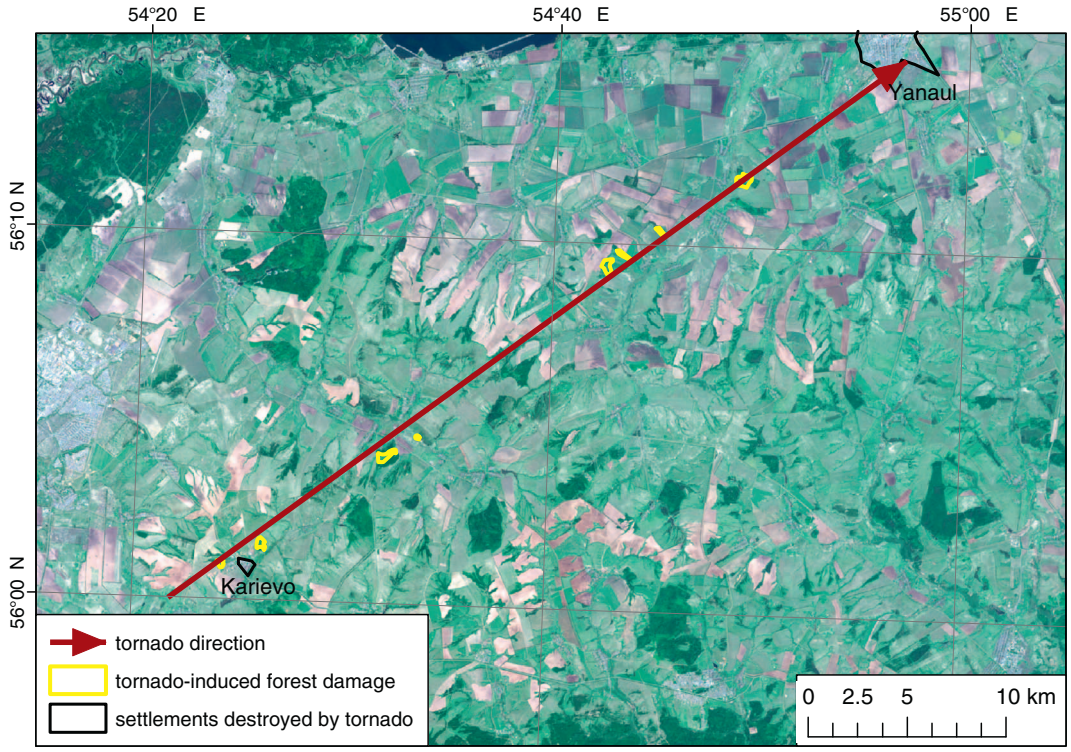

Fig. 11. Path of the F3 tornado that passed through in Bashkortostan Republic on 29 August 2014. Red arrow represents the tornado path (Chernokulsky et al., 2015). Tornado damage track is shown in yellow on the Landsat-8 image obtained on 22 May 2015. (For interpretation of the references to colour in this figure legend, the reader is referred to the web version of this article.)

time. Our results indicate that some forested regions are characterised by a comparatively high tornado density, reaching almost four tornadoes per 10,000 km^2 (> 0.2 tornadoes per 10,000 km^2 per year) which is 2–3 times higher than previously reported density values (see Fig. 2a in Groenemeijer and Kuhne (2014)). These regions formed somewhat of a 'forest tornado alley' that stretches from southwest to northeast. Moreover, we found a large number of northern tornadoes; thus, 58 tornadoes occurred north of 60° N. The northernmost tornado was observed at 65.6° N.

The largest number of tornadoes occurred in 2009 (22 tornadoes in total, 8 strong tornadoes with FI ≥ 2). June is the most favourable month for tornado formation, including strong tornadoes and tornado outbreaks. More than a half of all identified tornadoes have path lengths < 10 km. Most tornado tracks have maximum and mean widths of around 200–300 m and 100–200 m, respectively. The most common direction for tornado movement is from southwest to northeast. A few tornadoes with long and wide paths were found (up to 80 km length and 2000 m width); four tornadoes likely had F3 minimal intensity. These events formed in the abnormally warm and moist airs of a cyclone warm sector and were characterised by critical values of tornadogenesis indices. The total damage of tornadoes to forests in NE is rather low compared with windstorm-induced or fire-related disturbances; the former equals 17,200 ha over 15 years.

Our results revealed the incompleteness of current knowledge regarding tornado occurrence in low-populated forested areas of NE. The obtained information on > 100 tornadoes that were missed by observers and eyewitnesses should be taken into account for proper evaluation of tornado formation risk. This is especially important in light of global warming that may lead to an intensification of convective processes (Brooks, 2013; Diffenbaugh et al., 2013; Kurgansky et al., 2013; Meredith et al., 2015). Nevertheless, we should emphasise, that the presented climatology is also incomplete. In particular, our method does not allow identification of weak tornadoes that did not cause any forest disturbances or produced path widths < 60 m. The analysis was restricted to the period 2000–2014 and we plan to expand the study using the Eastern Europe's forest cover change data for the period 1985–2000 (Potapov et al., 2015). Thus, the true density of tornadoes in the forested regions of northeast Europe may be even higher, than presented here.

Acknowledgements

The authors thank three anonymous reviewers for their helpful comments, which have greatly improved the manuscript. We also thank Prof. Michael Kurgansky for fruitful and helpful discussions and Andrey Tarasov for helping with satellite data processing. The study was supported by the Russian Foundation for Basic Research (projects no. 15-35-20962-mol_a_ved and 16-05-00245-a) and projects of the RF President (MK-4513.2016.5 and MK-801.2017.5). Analysis of tornado intensities was supported by the Russian Science Foundation (project no. 14-17-00806).

Appendix A. Supplementary data

Supplementary data to this article can be found online at https://doi.org/10.1016/j.rse.2017.10.002.

References

Anderson, C., Wikle, C., Zhou, Q., Royle, J., 2007. Population influences on tornado reports in the United States. Weather Forecast. 22, 571–579.

Antonescu, B., Schultz, D.M., Lomas, F., Kühne, T., 2016. Tornadoes in Europe: synthesis of the observational datasets. Mon. Weather Rev. 144, 2445–2480. http://dx.doi.org/10.1175/MWR-D-15-0298.1.

Arino, O., Bicheron, P., Achard, F., Latham, J., Witt, R., Weber, J.-L., 2008. GlobCover: the most detailed portrait of Earth. In: European Space Agency Bulletin. 136. pp. 24–31.

Baumann, M., Ozdogan, M., Wolter, P.T., Krylov, A.M., Vladimirova, N.A., Radeloff, V.C., 2014. Landsat remote sensing of forest windfall disturbance. Remote Sens. Environ. 143, 171–179.

Bech, J., Gayà, M., Aran, M., Figuerola, F., Amaro, J., Arús, J., 2009. Tornado damage

analysis of a forest area using site survey observations, radar data and a simple analytical vortex model. Atmos. Res. 93 (1–3), 118–130.
Beck, V., Dotzek, N., 2010. Reconstruction of near-surface tornado wind fields from forest damage. J. Appl. Meteorol. Climatol. 49, 1517–1537.
Blanchard, D.O., 1998. Assessing the vertical distribution of convective available potential energy. Weather Forecast. 13, 870–877.
Brooks, H.E., 2004. On the relationship of tornado path length and width to intensity. Weather Forecast. 19, 310–319.
Brooks, H.E., 2013. Severe thunderstorms and climate change. Atmos. Res. 123, 129–138.
Chen, H., Chandrasekar, V., 2016. Real-time tornado detection and wind retrieval with high-resolution X-band Doppler radar network. In: International Geoscience and Remote Sensing Symposium (IGARSS), Art. No. 7729555, pp. 2150–2153. http://dx.doi.org/10.1109/IGARSS.2016.7729555.
Chernokulsky, A.V., Bulygina, O.N., Mokhov, I.I., 2011. Recent variations of cloudiness over Russia from surface daytime observations. Environ. Res. Lett. 6 (3), 035202.
Chernokulsky, A.V., Kurgansky, M.V., Zakharchenko, D.I., Mokhov, I.I., 2015. Genesis environments and characteristics of the severe tornado in the South Urals on August 29, 2014. Russ. Meteorol. Hydrol. 40, 794–799.
Coleman, T.A., Dixon, P.G., 2014. An objective analysis of tornado risk in the United States. Weather Forecast. 29, 366–376.
Davies-Jones, R.P., Burgess, D.W., Foster, M., 1990. Test of helicity as a forecast parameter. In: Preprints, 16th Conf. on Severe Local Storms. Amer. Meteor. Soc, Kananaskis Park, AB, Canada, pp. 588–592.
Diffenbaugh, N.S., Scherer, M., Trapp, J., 2013. Robust increases in severe thunderstorm environments in response to greenhouse forcing. Proc. Natl. Acad. Sci. U. S. A. 110, 16361–16366.
Doswell, C.A., Burgess, D.W., 1988. On some issues of United States tornado climatology. Mon. Weather Rev. 116, 495–501.
Doswell, C.A. III, Schultz, D.M., 2006. On the use of indices and parameters in forecasting severe storms. Electron. J. Severe Storms Meteorol. 1, 1–14.
Dotzek, N., Groenemeijer, P., Feuerstein, B., Holzer, A.M., 2009. Overview of ESSL's severe convective storms research using the European Severe Weather Database ESWD. Atmos. Res. 93, 575–586.
Dyer, R.C., 1988. Remote sensing identification of tornado tracks in Argentina, Brazil, and Paraguay. Photogramm. Eng. Remote. Sens. 54, 1429–1435.
Feuerstein, B., Dotzek, N., Grieser, J., 2005. Assessing a tornado climatology from global tornado intensity distributions. J. Clim. 18 (4), 585–596.
Finch, J., Bikos, D., 2012. Russian tornado outbreak of 9 June 1984. Electron. J. Severe Storms Meteorol. 7, 1–28.
Fujita, T.T., 1981. Tornadoes and downbursts in the context of generalized planetary scales. J. Atmos. Sci. 38, 1511–1534.
Godfrey, C.M., Peterson, C.J., 2017. Estimating enhanced Fujita scale levels based on forest damage severity. Weather Forecast. 32, 243–252. http://dx.doi.org/10.1175/WAF-D-16-0104.1.
Goliger, A.M., Milford, R.V., 1998. A review of worldwide occurrence of tornadoes. J. Wind Eng. Ind. Aerodyn. 74, 111–121.
Groenemeijer, P., Kuhne, T., 2014. A climatology of tornadoes in Europe: results from the European severe weather database. Mon. Weather Rev. 142, 4775–4790.
Hansen, M.C., Potapov, P.V., Moore, R., Hancher, M., Turubanova, S.A., Tyukavina, A., Thau, D., Stehman, S.V., Goetz, S.J., Loveland, T.R., Kommareddy, A., Egorov, A., Chini, L., Justice, C.O., Townshend, J.R.G., 2013. High-resolution global maps of 21st-century forest cover change. Science 342, 850–853.
Holland, A.P., Riordan, A.J., Franklin, E.C., 2006. A simple model for simulating tornado damage in forests. J. Appl. Meteorol. Climatol. 45, 1597–1611.
Jedlovec, G.J., Nair, U., Haines, S.L., 2006. Detection of storm damage tracks with EOS data. Weather Forecast. 21, 249–267.
Karstens, C.D., Gallus Jr., W.A., Lee, B.D., Finley, C.A., 2013. Analysis of tornado-induced tree fall using aerial photography from the Joplin, Missouri, and Tuscaloosa-Birmingham, Alabama, tornadoes of 2011. J. Appl. Meteorol. Climatol. 52, 1049–1068.
Klemp, J.B., 1987. Dynamics of tornadic thunderstorms. Annu. Rev. Fluid Mech. 19, 369–402.
Koroleva, N.V., Ershov, D.V., 2012. Estimation of error in determining the forest windfall disturbances area on high spatial resolution space images of LANDSAT-TM. In: Current Problems in Remote Sensing of the Earth From Space. 9. pp. 80–86 (in Russian).
Kramer, K., Brang, P., Bachofen, H., Bugmann, H., Wohlgemuth, T., 2014. Site factors are more important than salvage logging for tree regeneration after wind disturbance in Central European forests. For. Ecol. Manag. 331, 116–128.
Kurgansky, M.V., Chernokulsky, A.V., Mokhov, I.I., 2013. The tornado over Khanty-Mansiysk: an exception or a symptom? Russ. Meteorol. Hydrol. 38, 539–546.
Lehmann, J., Coumou, D., Frieler, K., Eliseev, A.V., Levermann, A., 2014. Future changes in extratropical storm tracks and baroclinicity under climate change. Environ. Res. Lett. 9, 084002.
Meredith, E.P., Semenov, V.A., Maraun, D., Park, W., Chernokulsky, A.V., 2015. Crucial role of Black Sea warming in amplifying the 2012 Krymsk precipitation extreme. Nat. Geosci. 8, 615–619.
Molthan, A.L., Bell, J.R., Cole, T.A., Burks, J.E., 2014. Satellite-based identification of tornado damage tracks from the 27 April 2011 severe weather outbreak. J. Oper. Meteorol. 2, 191–208.
Myint, S.W., Yuan, M., Cerveny, R.S., Giri, C., 2008. Comparison of remote sensing image processing techniques to identify tornado damage areas from Landsat TM data. Sensors 8, 1128–1156.
National Atlas of Russia, 2009. In: Borodko, A.V. (Ed.), Population and Economy. vol. 3. pp. 495. http://national-atlas.ru/ (in Russian).
Pisnichenko, I.A., 1994. The role of vapor-water phase transitions in the generation of tornadoes. Izv. Atmos. Oceanic Phys. 29 (6), 761–765.
Potapov, P.V., Turubanova, S.A., Hansen, M.C., 2011. Regional-scale boreal forest cover and change mapping using Landsat data composites for European Russia. Remote Sens. Environ. 115, 548–561.
Potapov, P.V., Turubanova, S.A., Hansen, M.C., Adusei, B., Broich, M., Altstatt, A., Mane, L., Justice, C.O., 2012. Quantifying forest cover loss in Democratic Republic of the Congo, 2000–2010, with Landsat ETM + data. Remote Sens. Environ. 122, 106–116.
Potapov, P.V., Turubanova, S.A., Tyukavina, A., Krylov, A.M., McCarty, J.L., Radeloff, V.C., Hansen, M.C., 2015. Eastern Europe's forest cover dynamics from 1985 to 2012 quantified from the full Landsat archive. Remote Sens. Environ. 159, 28–43.
Recommendation on Tornado Characteristics Estimate for Nuclear Energy Objects Usage, 2002. RB-022-1/Bulletin of Gosatomnadzor of Russia. (N.1. P.59-90. (in Russian)).
Rosencrants, T.D., Ashley, W.S., 2015. Spatiotemporal analysis of tornado exposure in five US metropolitan areas. Nat. Hazards 78, 121–140.
Saha, S., et al., 2010. The NCEP climate forecast system reanalysis. Bull. Am. Meteorol. Soc. 91, 1015–1057.
Sayn-Wittgenstein, L., Wightman, J.M., 1975. Landsat application in Canadian forestry. In: Proceeding of the 10th Int Symp on Remote Sensing of Environment. 2. pp. 1209–1218.
Schaefer, J.T., Edwards, R., 1999. The SPC tornado/severe thunderstorm database. In: Preprints, 11th Conf. on Applied Climatology. Amer. Meteor. Soc, Dallas, TX Available online at. https://ams.confex.com/ams/99annual/abstracts/1360.htm (6.11).
Silverman, B.W., 1986. Density Estimation for Statistics and Data Analysis. Chapman and Hall, New York (22 pp.).
Snitkovskiy, A.I., 1987. Tornadoes in the USSR. Meteorol. Gidrol. 9, 12–25 (in Russian).
Taszarek, M., Czernecki, B., Walczakiewicz, S., Mazur, A., Kolendowicz, L., 2016. An isolated tornadic supercell of 14 July 2012 in Poland – a prediction technique within the use of coarse-grid WRF simulation. Atmos. Res. 178–179, 367–379.
Timazhev, A.V., 2016. Frequency of blocking anticyclones in the Northern Hemisphere from RIHMI data: interannual variability. WCRP Rep.15/2016. In: Astakhova, E. (Ed.), Research Activities in Atmospheric and Oceanic Modelling. WMO, Geneva.
Vasil'ev, A.A., Peskov, B.E., Snitkovskiy, A.I., 1985. Tornadoes, squalls and hail of 8–9 June 1984. Sov. Meteorol. Hydrol. 8, 1–9.
Voznyachuk, L.N., 1954a. Revisiting question on the northern boundary of tornado propagation in Europe and Siberia. Bull. Belarus' State Univ. 21, 87–103 (in Russian).
Voznyachuk, L.N., 1954b. Materials for the study of tornadoes in Belarus. Bull. Belarus' State Univ. 21, 104–119 (in Russian).
Yuan, M., Dickens-Micozzi, M., Magsig, M.A., 2002. Analysis of tornado damage tracks from the 3 May tornado outbreak using multispectral satellite imagery. Weather Forecast. 17, 382–398.